International Journal of Heat and Mass Transfer 104 (2017) 400–408

Contents lists available at ScienceDirect

International Journal of Heat and Mass Transfer

journal homepage: www.elsevier.com/locate/ijhmt

Enhancement of thermal performance of micro heat pipes using wettability gradients

Manjinder Singh [a], Sasidhar Kondaraju [b], Supreet Singh Bahga [a,*]

[a] Department of Mechanical Engineering, Indian Institute of Technology Delhi, Hauz Khas, New Delhi 110016, India
[b] School of Mechanical Sciences, Indian Institute of Technology Bhubaneswar, Bhubaneswar, Orrisa 751013, India

ARTICLE INFO

Article history:
Received 23 April 2016
Received in revised form 17 July 2016
Accepted 19 August 2016

Keywords:
Micro heat pipe
Mixed wettability
Surface treatment
Heat transfer enhancement

ABSTRACT

We present a methodology for enhancing thermal performance of micro heat pipes (MHPs) by creating wettability gradients on the inner surface of MHPs. We analyse the effect of wettability gradients on MHP performance using a quasi one-dimensional mathematical model that accounts for axially-varying solid–liquid contact angle. For our analysis, we consider MHPs with various wettability schemes, such as uniform, step-variation, and linear variation in the contact angle. Our model predictions show that increasing the wettability of the evaporator surface and reducing the wettability of the condenser surface of MHP can lead to an increase in the heat transfer capacity of MHP by over 35%. We demonstrate the favourable effect of wettability gradients on MHP performance for different working fluids over a wide range of operating temperature and fluid charge. We also discuss the underlying physical mechanism that leads to enhanced thermal performance of MHP with mixed wetting surfaces. We show that the optimal choice of wettability gradient in MHP is governed by the competing effects of high liquid flow resistance in the lower wetting condenser and high liquid mass in the higher wetting evaporator.

1. Introduction

Continuous miniaturisation of electronics and increase in integration levels pose challenges in thermal management of microelectronic components [1,2]. As the failure rate of microelectronic chips increases exponentially with the operating temperature [2], cooling of chips is essential to ensure reliable operation. Micro heat pipes (MHPs) offer an efficient means of passively removing heat of order 10 W/cm^2 from microelectronic equipment using phase change phenomenon [3–5].

A typical MHP consists of a channel with sharp edges filled with a working fluid. The sharp edges of the heat pipe allow liquid flow due to capillary action, while the vapour flows through the inner core of channel. Fig. 1 shows a typical triangular cross-section MHP consisting of evaporator, adiabatic, and condenser sections. Heat input to the evaporator section vaporises the working fluid. The local increase in vapour pressure in the evaporator section drives the vapour to relatively cooler condenser section. The vapour condenses back to liquid in the condenser section and rejects the latent heat. The loss of liquid in the evaporator section results in reduced radius of curvature of the liquid meniscus. Whereas, the increase of liquid in the condenser section causes the local radius of curvature of meniscus to increase. Consequently, a pressure gradient develops in the liquid which drives the liquid from the condenser to the evaporator section, thereby completing the cycle. Although MHPs offer a reliable and passive chip cooling solution, MHP arrays in their current state can only transfer heat of order 10 W/cm^2 [6]. Therefore, any further improvement in the maximum heat transfer capacity of MHPs will help in dealing with growing challenges of thermal management of microelectronics.

The maximum heat transport capacity of an MHP depends on its geometry, working fluid, and the wettability of its inner surface. Since MHP relies on capillarity to transfer liquid from condenser to evaporator section, variation in geometry can strongly affect the performance of MHP. The capillarity of MHP can be enhanced by making the corners of MHP small and sharp. However, the reduced size of corners leads to higher hydraulic resistance to the liquid flow. Therefore, as discussed by Ma and Peterson [7], there exists an optimal geometry of MHP governed by the competing effects of capillary action and hydraulic resistance. Using an experimentally validated mathematical model, Ma and Peterson [7] showed that, for an MHP, an optimal groove size exists below which increased hydraulic resistance deteriorates its maximum heat transport capacity. Whereas, for groove size larger than the optimal size, reduced hydraulic resistance is unable to compensate

* Corresponding author.
E-mail address: bahga@mech.iitd.ac.in (S.S. Bahga).

http://dx.doi.org/10.1016/j.ijheatmasstransfer.2016.08.062
0017-9310/

Nomenclature

$\bar{u}$	mean velocity
$\dot{m}$	mass flow rate
A	flow area
$a/2$	groove side length
D	hydraulic diameter
fRe	Poiseuille number
h_{fg}	latent heat of vaporisation
L	length
N	number of grooves
p	pressure
Q	heat rate
R	half of the hydraulic diameter
r	radius of curvature
Re_c	radial Reynolds number in condenser section
Re_e	radial Reynolds number in evaporator section
x	distance from beginning of the evaporator section

Greek symbols

γ	half of apex angle of groove
μ	viscosity
ρ	density
σ	surface tension
θ	contact angle

Subscripts

a	adiabatic section
b	liquid block
c	condenser section
e	evaporator section
eff	effective
in	input
l	liquid
max	maximum
min	minimum
v	vapour

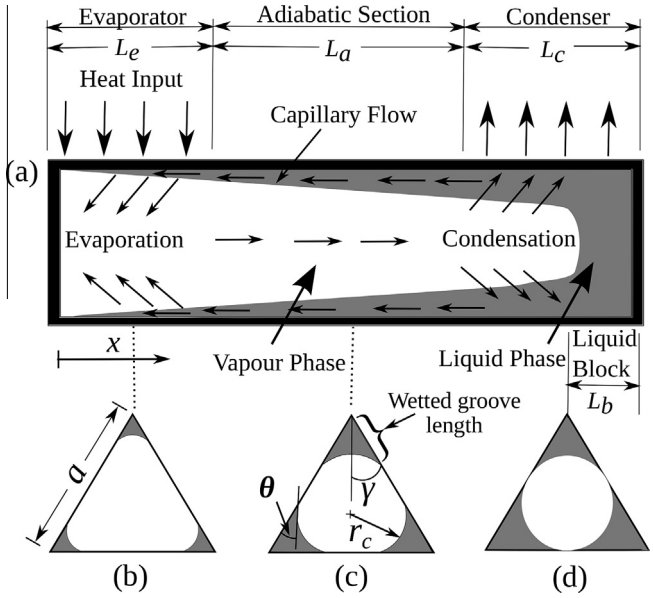

Fig. 1. Schematic illustrating operation of an MHP with triangular cross-section. (a) Heat input to the evaporator section causes the liquid in the corners of evaporator section to evaporate. The increased vapour pressure in the evaporator section drives the vapour to the condenser via the adiabatic section. The vapour condenses to liquid in the condenser section and rejects the latent heat. The increased amount of liquid in the condenser section (d) leads to larger radius of curvature of liquid meniscus compared with that in the evaporator (b) and the adiabatic sections (c). Consequently, an axial gradient in capillary pressure develops which drives the liquid back to the evaporator, thereby completing the working cycle of MHP.

for reduced capillary pumping. Here, we note that the optimal geometry of MHP is specific to the working fluid and the wettability of inner surface.

Another way of improving the heat transport capacity of an MHP is by using the right working fluid [8,9]. The operating characteristics of MHP depends on the thermo-physical properties of the working fluid, such as surface tension σ, liquid density ρ_l, latent heat of vaporisation h_{fg} and liquid viscosity μ_l. The effectiveness of the working fluid in MHP is usually characterised by a dimensional constant $(\sigma\rho_l h_{fg})/\mu_l$, termed as the Merit number [8]. The Merit number can be considered as a product of two terms, σ/μ_l and $\rho_l h_{fg}$. The first term σ/μ_l has the dimension of velocity and can be interpreted as the circulation rate of the working fluid [10]. Whereas, $\rho_l h_{fg}$ is the latent heat of evaporation per unit volume. Therefore, higher Merit number for a working fluid indicates better performance of the heat pipe. The thermo-physical properties of the working fluid and hence the Merit number are strongly dependent on the operating temperature. This affects the choice of working fluid for heat pipes operating at different working temperatures. For example, based on the Merit number, Reay and Kew [8] have shown that for operating temperatures below 323 K ammonia as a working fluid yields better performance than water. Whereas, water is preferable over ammonia as the working fluid above 323 K.

Besides the MHP geometry and working fluid, the heat transport capacity of MHP can also be increased by changing the wettability of inner surface of MHP. As shown experimentally by Wu and Peterson [11] and theoretically by Khrustalev and Faghri [12], the performance of MHP is enhanced if the working fluid wets the inner surface of MHP. This is because the capillarity increases when the liquid–vapour interface makes smaller contact angle with the solid surface. Most of the studies on the effect of wettability of surface on MHP performance have been limited to the case where the MHP surface has axially uniform wettability [9,12–15]. Recently, Hu et al. [16] experimentally demonstrated that heat pipes with axially varying wettability can yield enhanced heat transport capacity, compared with heat pipes with axially uniform wettability. Hu et al. chemically treated the inner surface of a grooved heat pipe to create a step variation of contact angle in evaporator, adiabatic, and condenser sections. Based on their experiments with water as the working fluid, Hu et al. [16] demonstrated that the heat pipe with a positive contact angle gradient from evaporator to condenser section (that is, higher wetting evaporator and lower wetting condenser), outperforms the heat pipe with uniformly higher wetting inner surface.

Using wettability gradients in MHP is particularly interesting because it can yield enhanced heat transport capacity over and above the thermal performance obtained by optimising MHP geometry and selection of appropriate working fluid. Moreover, wettability gradients can be generated on a variety of surfaces, such as using alkali surface oxidation [17] and laser etching [18] of copper, silane diffusion [19,20] on silicon wafers, and contact printing of octadecyltrichlorosilane [21] on oxidised silicon wafers.

Improved performance of heat pipe with higher wetting evaporator and lower wetting condenser can be qualitatively explained as the working liquid prefers to move to higher wetting evaporator, thereby prolonging dry-out. Hu et al. [16] gave similar qualitative arguments to explain improvement of heat transport capacity in their experiments on grooved heat pipes with wettability gradient. However, to best of our knowledge, we know of no theoretical model which quantifies the effect of wettability gradient on heat transfer performance of an MHP. Such a model will help in elucidating the physical mechanism governing the enhancement of heat transport capacity of MHPs with wettability gradient. Moreover, mathematical modelling of MHP with axially-varying contact angle can provide the optimal wettability gradient for maximising heat transport capacity of the MHP.

To this end, we present a one-dimensional mathematical model to investigate the effect of wettability gradients on the steady state performance of an MHP. Our model accounts for axial variations in solid–liquid contact angle and corresponding variation in the friction factor. Moreover, our model takes into account the temperature dependence of thermo-physical properties of working fluid. We validate our model with published experimental data [11] on operating characteristics of MHP with axially uniform wettability. Thereafter, we quantify the effect of wettability gradient on performance of MHP by considering several strategies of varying contact angle along the MHP axis, including step and linear variation. Importantly, we elucidate the physical mechanism underlying the enhancement of heat transport capacity of MHP with higher wetting evaporator and lower wetting condenser. Our model predictions show that MHPs with wettability gradients can yield enhanced thermal performance for different working fluids and operating temperatures compared with similar MHPs with uniformly wetting inner surface.

2. Mathematical modelling

We present a one-dimensional mathematical model to analyse the effect of wettability gradients on steady-state characteristics of a regular-polygonal shaped MHP with N corners. Here, we focus on the capillary limit which typically limits the performance of an MHP [22]. The contact angles used in the present study are relatively small (10° to 50°) and hence both evaporation and condensation occur in the filmwise mode in the MHP. As shown by the previous studies [23–25], surface wettability does not have a significant effect on the evaporation and condensation processes for the contact angle magnitudes between 10° and 50°. Hence we did not consider the effect of wettability on evaporation and condensation in the present model. For our analysis, we make several simplifying assumptions that are routinely employed while modelling thermal performance of MHPs [10,14,26,27]. Firstly, we assume that the operating temperature is axially uniform. This assumption is reasonable as axial variation in temperature of a typical MHP is around 1 K [27,14] owing to high conductance of MHP. Moreover, we assume that the liquid and vapour phases are at saturated conditions [26] corresponding to the operating temperature. We also assume that the uniform heat flux is distributed identically among all the corners of MHP. Consequently, the working liquid is distributed evenly among all the corners of MHP.

For axially-uniform heat flux along the evaporator and condenser section, the dependence of heat transport rate $Q(x)$ on the axial distance x from the beginning of the evaporator section ($x = 0$) is given by

$$Q(x) = \begin{cases} \frac{x}{L_e} Q_{in}, & 0 \leqslant x \leqslant L_e \\ Q_{in}, & L_e \leqslant x \leqslant L_e + L_a \\ Q_{in}\left(1 + \frac{L_e + L_a - x}{L_{eff,c}}\right), & L_e + L_a \leqslant x \leqslant L_e + L_a + L_{eff,c}, \end{cases} \tag{1}$$

where Q_{in} denotes the total heat input and L denotes the length of corresponding sections of MHP. The subscripts e, a, and c denote evaporator, adiabatic and condenser sections, respectively. We note that $Q(x)$ is the net heat added to the MHP up to the distance x, and not the local heat input at location x. Therefore, $Q(x)$ is non-zero in the adiabatic section. In the above equation we have used the effective condenser length $L_{eff,c}$ instead of the actual condenser length L_c to account for the liquid block. As shown in the Fig. 1, the liquid block results due to the overcharging of MHP and resists heat transfer from vapour to condenser walls. The effective length of the condenser section in presence of liquid block of length L_b is given by

$$L_{eff,c} = L_c - L_b. \tag{2}$$

Under steady state conditions, the liquid and vapour mass flow rates at a given section are equal in magnitude. The mass flow rate of liquid and vapour at every section of the heat pipe can be obtained using energy balance [28] as

$$\dot{m}_l = -\dot{m}_v = \frac{Q(x)}{h_{fg}}, \tag{3}$$

where $\dot{m}$ is mass flow rate, h_{fg} is latent heat of vaporisation and subscripts l and v denote liquid and vapour phases, respectively. Knowing the mass flow rate of liquid and vapour, we can calculate the axial variation of pressure in liquid and vapour phases using the equations for momentum conservation. The pressure variation in liquid and vapour phases also depends on the liquid level in the MHP, which can be obtained by using the Young–Laplace equation to relate the pressure jump across the liquid–vapour interface with the curvature of liquid interface.

Liquid flow in an MHP is characterised by low Reynolds number ($Re \ll 1$), where inertial effects can be neglected. Moreover, long and slender geometry of the grooves through which liquid flows in an MHP ensure that the flow is quasi one-dimensional. The pressure in the liquid p_l is therefore given by the lubrication approximation of Navier Stokes equations [28],

$$\frac{dp_l}{dx} = \frac{2\mu_l f Re \dot{m}_l}{\rho_l A_l N D^2}, \tag{4}$$

where ρ and μ respectively denote the density and dynamic viscosity of the fluid, and fRe is the Poiseuille number defined as the product of friction factor and Reynolds number at the given cross-section. The Poiseuille number fRe is a function of solid–liquid contact angle, and therefore in this work we use the correlation derived from the numerical results of Ayyaswami et al. [29]. In Eq. (4), A_l denotes the local cross-sectional area of liquid in one groove and D denotes the corresponding hydraulic diameter. For a triangular corner with corner half-angle γ and contact angle θ as shown in Fig. 1(c), the liquid flow area A_l and hydraulic diameter D depends on the radius of curvature of the liquid–vapour meniscus r as (see Appendix A)

$$A_l = \beta r^2, \text{ where}$$
$$\beta = N\left[\cot(\gamma+\theta) - \left(\frac{\pi}{2} - (\gamma+\theta)\right) + \frac{\cot(\gamma+\theta)\cos(\gamma+\theta)\sin(\theta)}{\sin(\gamma)}\right], \tag{5}$$

$$D = \frac{A_l}{2r\cos(\gamma+\theta)}. \tag{6}$$

While arriving at Eq. (4), we have neglected the contribution of momentum change of liquid associated with evaporation and condensation, which is small compared with change in momentum of the bulk liquid. However, this assumption is not valid for vapour flow, as the momentum change associated with mass addition and removal due to phase change is not small compared with the

bulk momentum change of vapour. Moreover, unlike in liquid flow, the Reynolds number for vapour flow is not small. For a known heat input, the pressure drop in vapour flow inside a heat pipe taking into account the effects of evaporation and condensation has been modelled by Faghri et al. [30]. Here, we use the analytical expressions developed by Faghri et al. [30] for vapour pressure drop in various sections of the heat pipe,

$$\frac{dp_v}{dx} = \begin{cases} 2\left(-8|Re_e| - \frac{16}{3}Re_e^2\right)\left(\frac{\mu_v^2}{\rho_v R^4}\right)x, & 0 \leqslant x \leqslant L_e \\ \left(\frac{-8\mu_v \bar{u}_{v,a}}{R^2}\right), & L_e \leqslant x \leqslant L_e + L_a \\ 2\left(-8|Re_c| - \frac{16}{3}Re_c^2\right)\left(\frac{\mu_v^2}{\rho_v R^4}\right)x & \\ \quad +\left(\frac{16}{3}|Re_c| - 8\right)\left(\frac{\mu_v \bar{u}_{v,a}}{R^2}\right), & L_e + L_a \leqslant x \leqslant L_e + L_a + L_{eff,c}, \end{cases} \tag{7}$$

where R represents half of the hydraulic diameter of vapour region. The hydraulic diameter is defined as four times the ratio of vapour flow area and perimeter of the cross section of the vapour region. In this equation, Re_e and Re_c are dimensionless numbers respectively denoting radial Reynolds number in evaporator and condenser section, and $\bar{u}_{v,a}$ is the mean vapour flow velocity in the adiabatic section,

$$Re_e = \frac{\dot{m}_{v,a}}{2\pi L_e \mu_v}, \quad Re_c = \frac{\dot{m}_{v,a}}{2\pi L_c \mu_v}, \quad \bar{u}_{v,a} = \frac{\dot{m}_{v,a}}{\rho_v \pi R^2}. \tag{8}$$

During the operation of MHP, the mass of working liquid in the evaporator section decreases, while that in the condenser increases. The maximum heat transport capacity of an MHP corresponds to the heat input at which the evaporator section drys out. Therefore, it is necessary to obtain the mass distribution of liquid in the MHP. The amount of liquid present in the MHP at any section depends on the local cross-sectional area of the liquid, which in turn depends on the radius of curvature of liquid–vapour interface r through Eq. (5). The axial variation of the radius of curvature of interface can be obtained by relating it with pressure jump across the liquid–vapour interface, using the Young–Laplace equation

$$p_v - p_l = \frac{\sigma}{r}, \tag{9}$$

where, σ denotes the surface tension of the liquid. Here, we have neglected the axial principal radius of curvature as it is significantly smaller than the lateral principal radius of curvature r, shown schematically in Fig. 1. Next, differentiating Eq. (9) with respect to x we obtain a differential equation for axial variation of interface curvature,

$$\frac{dr(x)}{dx} = \frac{r(x)^2}{\sigma}\left(\frac{dp_l}{dx} - \frac{dp_v}{dx}\right). \tag{10}$$

To solve Eq. (10) for a given heat input Q_{in}, we first calculate liquid and vapour mass flow rates using Eq. (3). We then calculate the pressure gradients in liquid and vapour phases using Eqs. (4) and (7). Finally, we integrate Eq. (10) to obtain the axial variation of interface curvature. In practice, we solve Eq. (10) numerically using the fourth-order Runge–Kutta scheme in a domain (length of the MHP) discretized with 5700 grid points. We note that solution of Eq. (10) requires the value of radius of curvature at the beginning of evaporator, $r(0) = r_{min}$. The value of r_{min} can be chosen iteratively such that the total mass of working fluid is equal to actual fluid charge of MHP. In certain cases, the value of radius of curvature in the condenser section can exceed the maximum value r_{max} at which the liquid completely wets the groove. This maximum radius of curvature is given by (see Appendix A),

$$r_{max} = \frac{a}{2}\frac{\sin(\gamma)}{\cos(\gamma + \theta)}, \tag{11}$$

where $a/2$ is the length of groove as shown in Fig. 1. If the radius of curvature exceeds r_{max} at a particular location we assume that, beyond this location, a liquid block fills the condenser. Lastly, the maximum heat transport capacity Q_{max} of the MHP is given by that value of heat input Q_{in} for which the radius of curvature of interface at the beginning of evaporator $r(0)$ attains a vanishingly small value. Because substitution of $r = 0$ in Eq. (10), leads to a singularity in the right hand side of Eq. (10), we choose a very small value of r_{min} to solve for the dry-out condition. For our calculations we choose the minimum radius of curvature at dry-out as $r_{min} = 0.02 \times r_{max}$. Our calculations show that choosing a smaller value of r_{min} than $0.02 \times r_{max}$ at dry-out does not affect the value of maximum heat transport capacity Q_{max} of MHP.

3. Results and discussion

To highlight the effect of wettability gradient on the steady state performance of MHPs, we solved the governing equation (Eq. (10)) for a trapezoidal MHP by considering different wettability gradients. For our calculations, we considered a trapezoidal shaped MHP having geometric parameters given in Table 1 and water as the working fluid. The geometrical parameters given in Table 1 correspond to the MHP used in the experimental work by Wu and Peterson [11]. Previous experimental and modelling studies on the MHP with these geometric parameters have shown that the steady state thermal performance of this MHP is limited by the capillary limit [22]. Therefore, in the current work we focus only on the capillary limit of MHP. We analysed the effect of five wettability gradients, including uniform, step variation, and linear variation of contact angle (shown in Table 2) on the performance of this MHP for varying operating temperatures and the fluid charge. In addition, we performed calculations for maximum heat transport capacity of MHP for uniform contact angle of 55° to validate our model with experimental results of Wu and Peterson [11] for the same MHP. Lastly, we consider the effect of different working fluids, such as ammonia, heptane, methanol, and acetone on the heat transfer capacity of the MHP in presence of wettability gradients. For all our calculations, we used thermophysical properties of working fluids from NIST chemistry webbook [31]. Until and unless specified, throughout the discussion in the paper, sections of MHP with contact angle of 10° and 50° are respectively termed as higher and lower wetting surfaces. The MHP with uniform contact angle

Table 1
Geometrical parameters of the MHP used in the current work.

Parameter	Value unit
Evaporator section length, L_e	13 mm
Adiabatic section length, L_a	31 mm
Condenser section length, L_c	13 mm
Groove side length, $a/2$	0.33 mm
Half angle, γ	30°
Number of grooves, N	4

Table 2
Wettability schemes used in the current work to illustrate the effect of wettability gradients on thermal performance of MHP.

Wettability scheme	Contact angle (θ)		
	Evaporator	Adiabatic	Condenser
Uniform 50°	50°	50°	50°
Uniform 10°	10°	10°	10°
Step variation 10°–50°–50°	10°	50°	50°
Step variation 10°–10°–50°	10°	10°	50°
Linear variation 10°–50°	10° in evaporator to 50° in condenser		

of 10° is termed as higher wetting MHP, while the MHP with uniform contact angle of 50° is termed as lower wetting MHP.

3.1. Effect of wettability gradients on liquid distribution in MHP

We begin by considering the steady state distribution of working liquid in the MHP for different wettability schemes shown in Table 2. We performed calculations for operating temperature of 333 K, fluid charge of 1 mg and heat input of 0.08 W. Fig. 2(a) shows the axial variation of the radius of curvature of the liquid–vapour meniscus for different wettability schemes. At steady state, the radius of curvature of the meniscus increases monotonically along the MHP axis, as the liquid recedes from the evaporator section and accumulates in the condenser section. The radius of curvature of the meniscus increases steeply for the lower wetting MHP ($\theta = 50^{\circ}$), whereas the meniscus curvature varies gradually along the MHP axis for higher wetting MHP ($\theta = 10^{\circ}$). Such trends are expected, because the liquid spreads more on surfaces with higher wettability.

Another way of describing the difference in behaviour of lower wetting and higher wetting MHPs is by noting that, for same meniscus curvature, the liquid flow area $A_l = \beta r^2$ given by Eq. (5) is low when the contact angle is large. This is because, for same meniscus curvature, the wetted groove length, as shown in Fig. 1(c) is small for a large contact angle. The reduced liquid flow area for lower wetting MHP leads to higher liquid pressure drop for the same mass flow rate (and heat input) as shown in Fig. 2(b). Consequently, from Eq. (10), high liquid pressure gradient leads to steep axial variation of the meniscus curvature in the lower wetting MHP. Note that, the vapour pressure gradient shown in Fig. 2(b) is low compared with the liquid pressure gradient, and hence the former has minimal effect on the meniscus curvature. Importantly, the radius of curvature of the meniscus at the evaporator inlet is lowest for the MHP with lower wetting surface ($\theta = 50^{\circ}$). This suggests that the MHP with lower wetting surface ($\theta = 50^{\circ}$) is more prone to dry-out.

The model predictions for MHPs with step variation in wettability (10°–50°–50° and 10°–10°–50°) can be explained based on the above conclusions for uniformly wetting MHPs. As shown in Fig. 2(a), in MHPs with step change in contact angle, the radius of curvature of meniscus increases gradually in higher wetting sections and increases abruptly in sections with lower wetting surface. The abrupt increase in the radius of curvature of the meniscus results from reduced liquid flow area and correspondingly higher pressure

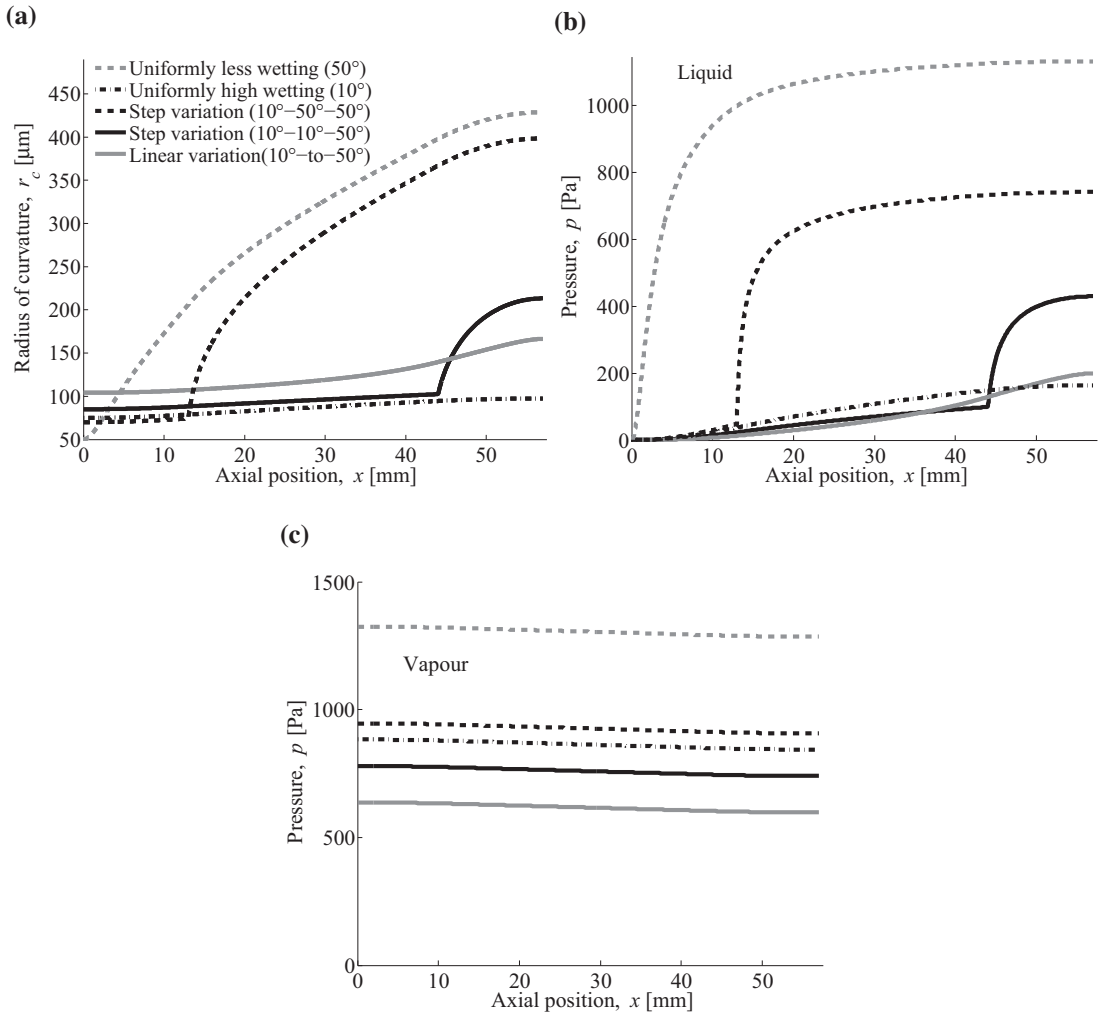

Fig. 2. Effect of surface wettability on liquid distribution and pressure in MHP. (a) Axial variation of the radius of curvature of liquid–vapour meniscus for different wettability schemes. Compared with uniformly higher wetting MHP 10°, the radius of curvature at the evaporator inlet ($x = 0$) is higher for MHPs with 10°–10°–50° and linear variation in the contact angle, suggesting that these wettability schemes are less prone to dry-out. Axial variation of (b) liquid and (c) vapour pressure for different wettability schemes. (b) The liquid pressure varies gradually in higher wetting sections compared with that in lower wetting sections. (c) The vapour pressure drop is small compared with liquid pressure drop, indicating that liquid pressure primarily dictates the operation of MHP. These calculations are based on 0.08 W heat input and 1 mg of water as the working fluid.

drop in the lower wetting sections of the MHP, as shown in Fig. 2 (b). The reduced flow area in the lower wetting sections of the MHP also leads to redistribution of working fluid to the higher wetting sections. For example, redistribution of working fluid from lower wetting to higher wetting sections in MHPs with wettability gradients (10°–10°–50° and linearly varying θ from 10° to 50°) leads to larger radius of curvature of the meniscus at the evaporator inlet compared with that in uniformly higher wetting MHP (uniform contact angle of 10°). The large quantity of working fluid in the evaporator section indicates better thermal performance as more heat can be added to the MHP before dry out occurs in the evaporator.

In general, the thermal performance of MHPs with higher wetting evaporator and lower wetting condenser is governed by the competing effects of high liquid flow resistance (and liquid pressure drop) in the lower wetting condenser and high liquid mass (and radius of curvature of meniscus) in the higher wetting evaporator. A comparison of the results presented in Fig. 2(a) and (b) shows that among the various wettability schemes considered here, linearly varying contact angle (10°–50°) and wettability gradient (10°–10°–50°) yields highest radius of curvature of the meniscus at the evaporator inlet and comparatively lower pressure drop. Therefore, the MHP with wettability gradient (10°–10°–50°) and linearly varying contact angle (10°–50°) are expected to show dry-out at higher input heat flux compared with other wettability schemes.

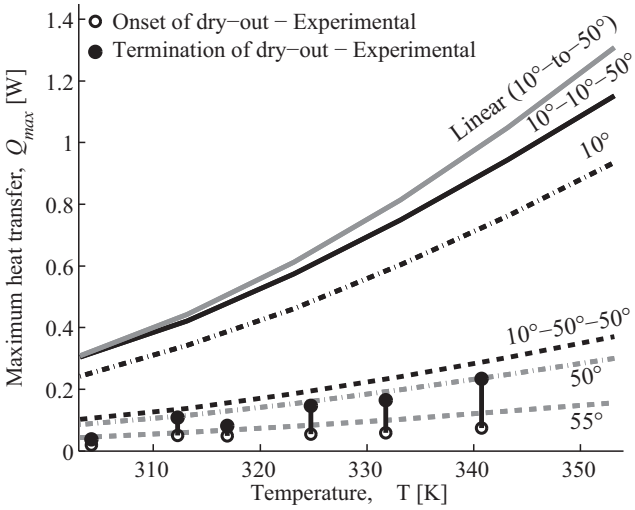

Fig. 3. Effect of surface wettability on the maximum heat transfer capacity of MHP at different operating temperatures. The MHPs with linear wettability gradient and step variation of 10°–10°–50° in contact angle show even better thermal performance than the MHP with uniformly higher wetting surface ($\theta = 10°$). Also shown are the experimental data of Wu and Peterson [11] for the case of MHP with contact angle of 55°. The lower and upper points in the experimental data denote the beginning and the end of dry-out, respectively. These calculations are based on 3.2 mg of water as the working fluid.

3.2. Effect of wettability gradients on maximum heat transfer rate of MHP

We now consider the effect of various wettability schemes, shown in Table 2, on the maximum heat transfer rate Q_{max} of the MHP. The maximum heat transfer capacity of the MHP is defined as the heat input at which dry-out first occurs at the evaporator inlet. That is, at dry-out, the radius of curvature of the meniscus at the evaporator inlet attains its minimum value. For our calculations, we assumed a dry-out condition of $r(0) = 0.02 \times r_{max}$, where r_{max} is the maximum radius of curvature of the meniscus given by Eq. (11). In Fig. 3, we present the maximum heat transfer rate of the MHPs with different wettability schemes at varying operating temperatures. For these calculations, we assumed that MHPs with different surface wettabilities contain equal mass (3.2 mg) of the working fluid. In Fig. 3, we also present experimental data of Wu and Peterson [11] for maximum heat transfer rate of copper MHP having same geometry, working fluid, fluid charge, and a uniform contact angle of 55°. The maximum heat transfer rate predicted by our model for MHP with uniform contact angle of 55° agrees well with the experimental data of Wu and Peterson [11]. Irrespective of the wettability scheme, the maximum heat transfer rate of MHP increases with the operating temperature, as shown in Fig. 3. This is because, for water as the working fluid, the Merit number $(\sigma\rho_l h_{fg})/\mu_l$ increases with the operating temperature [8].

Consistent with our discussion in Section 3.1, the results presented in Fig. 3 show that among MHPs with uniform wettability, the higher wetting MHP ($\theta = 10°$) shows better thermal performance compared with the lower wetting MHP ($\theta = 50°$) at all operating temperatures. The MHPs having wettability gradients with step variation of contact angle (10°–10°–50°) and linear variation of contact angle (10° in the evaporator to 50° in the condenser) show even higher heat transfer capacity than higher wetting MHP with $\theta = 10°$. For example, at an operating temperature of 333 K, treating the MHP for linear (10°–50°) and step (10°–10°–50°) variation in contact angle yields more than 35% and 25% increase in heat transfer capacity, respectively, compared with higher wetting MHP ($\theta = 10°$). Similarly, the MHP with 10°–50°–50° variation in contact angle shows better thermal performance than the lower wetting MHP ($\theta = 50°$). We note that the experimental data on thermal performance of heat pipes with wettability gradients is limited to that by Hu et al. [16] for grooved heat pipes. We know of no experimental study on evaluating the effect of wettability gradients on MHP performance with which we can quantitatively validate our calculations. However, we note that our modelling predictions for MHPs with wettability gradients are in qualitative agreement with experimental data of Hu et al. [16] for grooved heat pipes. In particular, the results presented in Fig. 3 show that MHP with hydrophobic condenser and hydrophilic evaporator can yield higher heat transfer capacity than a similar heat pipe with uniformly hydrophilic or hydrophobic inner surface.

In Fig. 4 we present the effect of fluid charge on maximum heat transfer capacity of MHPs with different wettability schemes, for a fixed operating temperature of 353 K. The inset plot in Fig. 4 shows the same data for schemes (10°–10°–50°) and linear variation (10°–50°), but for a wider range of fluid charge. For all wettability schemes considered here, the maximum heat transfer capacity increases with the fluid charge. However, at higher mass of working fluid (around $m = 3.2$ mg), the improvement in heat transfer capacity of heat pipes with uniformly less-wetting surface ($\theta = 50°$), uniformly high-wetting ($\theta = 10°$), and step variation 10°–50°–50° reduces with an increase in the mass of working fluid as shown in Fig. 4. This suggests that, the heat pipes with uniformly less-wetting surface ($\theta = 50°$), uniformly high-wetting ($\theta = 10°$), and step variation of 10°–50°–50° in contact angle attain their optimal fluid charging around $m = 3.2$ mg. This saturation of maximum heat transfer capacity can be attributed to the formation of liquid block in the condenser section when the MHP is loaded with an excess of working fluid.

The maximum heat transfer capacity for heat pipes with wettability gradient (10°–10°–50°) and linearly varying (10°–50°) also increases with the fluid charge, as shown in Fig. 4(b). However, due to redistribution of liquid from condenser to evaporator section due to hydrophilic evaporator and hydrophobic condenser leads to higher optimal fluid charge (around 8 mg). For a wide range of fluid charge (up to 4.2 mg) the heat pipe with linearly varying contact angle (10°–50°) has higher heat transfer capacity. However, at higher fluid charge, the heat pipe with (10°–10°–50°)

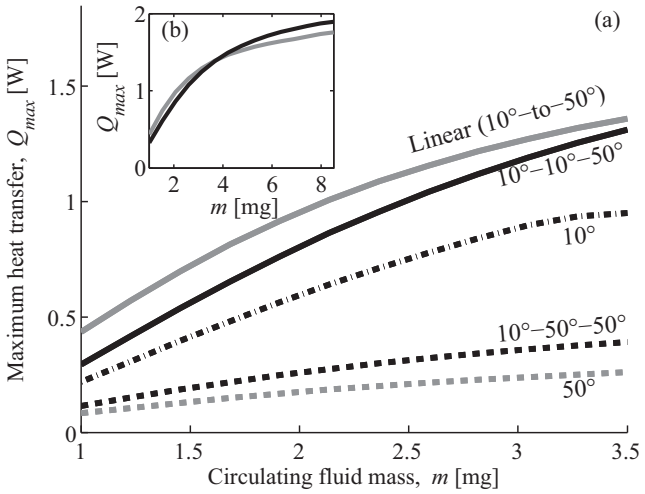

Fig. 4. Effect of surface wettability on the maximum heat transfer capacity of MHP for varying mass of working fluid. The improvement in thermal performance of MHP with an increase in fluid mass diminishes at higher mass of working fluid due to the formation of liquid block. The relative thermal performance of MHPs with different wettability gradients is same as that in Fig. 3 for the fluid charge range 0–4.2 mg. As shown in the inset, at higher mass of working fluid, 10°–10°–50° shows better thermal performance than the MHP linear (10°–50°) wettability gradient. These calculations were performed for operating temperature of 353 K.

variation in contact angle yields the highest heat transfer capacity. Notwithstanding the above change in order of best wettability scheme with an increase in fluid charge, the results presented in Figs. 3 and 4 confirm that MHPs having evaporator with higher wetting surface and condenser with lower wetting surface exhibit enhanced heat transfer capacity compared with MHPs with uniform surface wettability.

3.3. Effect of wettability gradients on MHP performance for different working fluids

Till now we have shown that MHPs with wettability gradients can lead to higher heat transfer capacity compared with MHPs with uniform wettability. However, our analysis was limited to MHPs using water as the working fluid. As the thermo-physical properties of the working fluid also affect the thermal performance of MHP [8], it is essential to evaluate the effect of wettability gradients on MHP performance for different working fluids. The relative effectiveness of different working fluids in MHPs can be characterised approximately by the Merit number; the variation of Merit number versus temperature for different working fluids is provided in Reay and Kew [8]. We note that, the Merit number does not account for the actual variation of meniscus curvature, and hence liquid and vapour pressures, along the MHP axis. Therefore, to evaluate the effect of thermophysical properties of working fluid on MHPs with different wettability gradients, it is necessary to calculate the maximum heat transfer capacity of MHPs, rather than relying solely on the Merit number. To this end, we calculate the maximum heat transfer capacity of MHPs with uniform contact angle ($\theta = 10^{\circ}$) and linearly varying contact angle (10° in evaporator to 50° in condenser), when charged separately with water, acetone, ammonia, heptane, and methanol. For these calculations, we assumed that the mass of working fluid is 3.2 mg.

Fig. 5(a) shows the predicted values of maximum heat transfer capacity of MHP with uniform wettability ($\theta = 10^{\circ}$) at various operating temperatures for different working fluids. For all working fluids, except ammonia, the maximum heat transfer capacity increases with the operating temperature as temperature dependence of their thermo-physical properties results in higher Merit

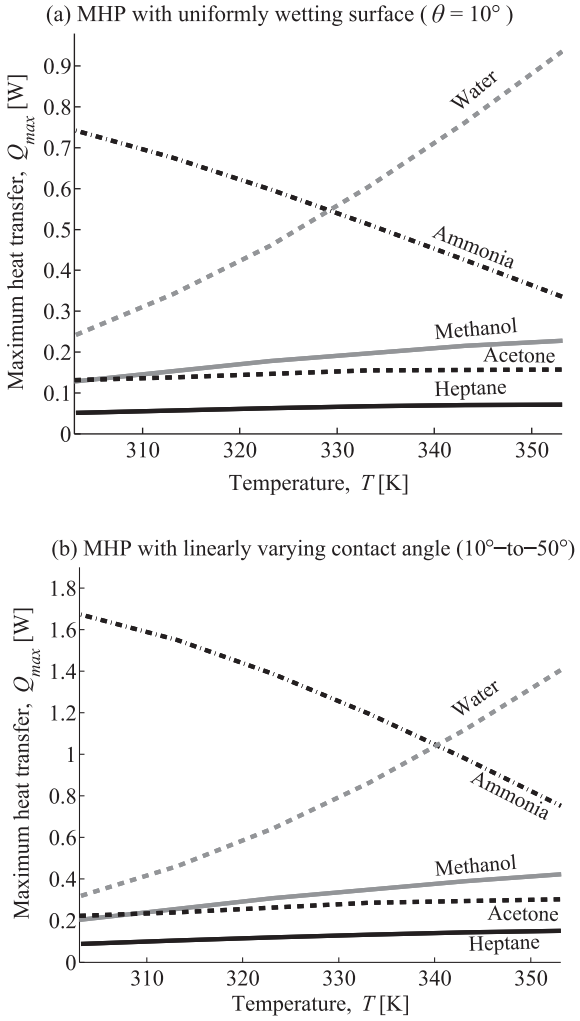

Fig. 5. Effect of wettability gradient on thermal performance of MHPs charged with different working fluids. (a) The maximum heat transfer capacity of MHP with uniform contact angle of 10° for varying operating temperatures. MHPs with ammonia and water show the best thermal performance below and above 328 K, respectively. (b) The maximum heat transfer capacity of MHP with linearly varying contact angle (10° in evaporator and 50° in condenser) for varying operating temperatures. For all working fluids, the MHP with linear wettability gradient yields better heat transfer capacity than that with uniformly higher wetting surface shown in (a). For these calculations, we assumed a fixed working fluid mass of 3.2 mg.

number $(\sigma\rho_l h_{fg})/\mu_l$ at higher temperatures. Whereas, the Merit number for ammonia decreases with an increase in temperature, and hence the maximum heat transfer capacity of MHP decreases with the operating temperature. The results shown in Fig. 5(a) suggest that ammonia is better suited as a working fluid below 328 K, above which water yields the highest heat transfer capacity.

When a wettability gradient is introduced in the MHP such that the constant angle varies linearly from 10° in the evaporator to 50° in the condenser section, the maximum heat transfer capacity of MHP increases for all working fluids (Fig. 5(b)). This suggests that, wettability gradients can be employed to enhance the thermal performance of MHPs and other heat pipes irrespective of the working fluid. The differential increase in heat transfer capacity for different working fluids also leads to a change in the temperature above which water becomes preferable working fluid over ammonia. For example, for linear wettability gradient (Fig. 5(b)), the temperature above which water becomes preferable working fluid over ammonia is 338 K compared with 328 K in the case of higher wetting MHP (Fig. 5(a)).

4. Conclusion

We have described a methodology for improving the thermal performance of MHPs by creating gradients in the wettability of inner surface of MHPs. To quantify the effect of wettability gradients on heat transfer capacity of MHPs, we have developed a one-dimensional mathematical model for MHP which accounts for axial variations in solid–liquid contact angle. We considered different wettability schemes, including uniform, step-variation, and linear variation in wettability of the inner surface of MHP. Our model predictions show that among the uniformly wetting MHPs, higher wettability surfaces show better thermal performance than the lower wetting surfaces. Interestingly, our calculations show that MHPs with higher wetting evaporator and lower wetting condenser can exhibit even better thermal performance than the MHP with corresponding uniformly higher wetting surface. Qualitatively, these trends are applicable over a wide range of operating temperature and mass of working fluid. We also showed that the enhancement in maximum heat transfer capacity of MHP due to wettability gradients occurs for a variety of working fluids such as water, ammonia, heptane, acetone, and methanol.

Based on our model predictions, we have also discussed the physical mechanism underlying enhanced thermal performance of MHPs with mixed wetting surfaces. We showed that increasing the wettability of evaporator surface and reducing the wettability of condenser surface causes the working fluid to redistribute from condenser to evaporator. This enables the MHP to sustain higher heat input before the evaporator dries out. However, making condenser and adiabatic sections highly less wetting leads to higher resistance to liquid flow, which can deteriorate the thermal performance of MHP. Therefore, the thermal performance of MHPs with mixed wetting surfaces is governed by the competing effects of high liquid flow resistance in the lower wetting condenser and high liquid mass in the higher wetting evaporator. Among the various wettability schemes considered in the current work, for a large range of fluid mass, linear variation in contact angle with higher wetting evaporator and lower wetting condenser yields the best thermal performance of MHP. In particular, compared with an equivalent MHP having uniformly higher wetting surface ($\theta = 10^\circ$), the MHP with linearly varying contact angle from 10° in evaporator to 50° in condenser shows over 35% increase in heat transfer capacity. However, we find that for high fluid mass the MHP with 10°–10°–50° variation in contact angle yields the best thermal performance among all the wettability schemes considered in this work. Here, we note that the wettability gradients schemes used in the current work are only for illustrating the effect of wettability gradient on enhancement of heat transfer in MHPs. To find the optimal wettability gradient which will yield the highest heat transfer in MHP would require detailed optimisation, which we will present in a future work. Finally, we note that, creating wettability gradients is a relatively less explored way of enhancing thermal performance of MHPs. Wettability gradients are particularly interesting because they can be employed for performance enhancement of MHPs over and above the improvement due to geometry optimisation and choice of proper working fluid.

Appendix A. Liquid cross-sectional area and maximum radius of curvature

Here, we provide the derivations for Eqs. (5) and (11) for the cross-sectional area of liquid flow and the maximum possible radius of curvature, respectively. Fig. A.6 shows the geometry of the cross-section of a groove filled with the liquid. From Fig. A.6, we have,

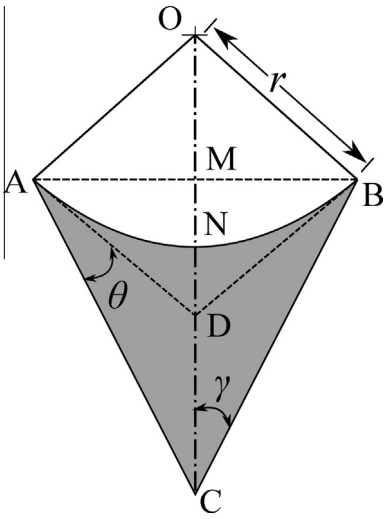

Fig. A.6. Geometry of cross-section of the liquid-filled groove of MHP.

$$\angle ACD = \gamma, \quad \angle DBC = \theta, \quad \angle CDB = \pi - (\gamma + \theta),$$
$$\angle ADB = 2(\gamma + \theta), \quad \angle AOB = \pi - 2(\gamma + \theta). \tag{A.1}$$

From $\triangle AOM$,

$$AM = r \sin\left(\frac{\pi}{2} - (\gamma + \theta)\right) = AC \sin(\gamma), \tag{A.2}$$

which simplifies to

$$r = AC \frac{\sin(\gamma)}{\cos(\gamma + \theta)}. \tag{A.3}$$

The radius of curvature of the meniscus reaches its maximum value when the groove with side-length $a/2$ is completely filled, which gives

$$r_{max} = \frac{a}{2} \frac{\sin\gamma}{\cos(\gamma + \theta)}. \tag{A.4}$$

To calculate the liquid flow area in a single groove (A_l'), we note from Fig. A.6 that,

$$A_l' = \text{Area of } ACBD + \text{Area of } \triangle ADB + \text{Area of } \triangle AOB - \text{Area of circular segment } ANB, \tag{A.5}$$

where,

$$\begin{aligned} &\text{Area of } ACBD = r^2 \frac{\cot(\gamma + \theta)\cos(\gamma + \theta)\sin(\theta)}{\sin(\gamma)}, \\ &\text{Area of } \triangle ADB = r^2 \cot(\gamma + \theta)\cos^2(\gamma + \theta), \\ &\text{Area of } \triangle AOB = r^2 \cos(\gamma + \theta)\sin(\gamma + \theta), \\ &\text{Area of circular segment } ANB = r^2\left(\frac{\pi}{2} - (\gamma + \theta)\right). \end{aligned} \tag{A.6}$$

Using these expressions in Eq. (A.5) we get

$$A_l' = r^2\left(\cot(\gamma + \theta) - \left(\frac{\pi}{2} - (\gamma + \theta)\right) + \frac{\cot(\gamma + \theta)\cos(\gamma + \theta)\sin(\theta)}{\sin(\gamma)}\right). \tag{A.7}$$

The total liquid flow area (A_l) in all the N grooves is given by $A_l = NA_l'$. That is,

$$A_l = \beta r^2, \quad \text{where}$$
$$\beta = N\left[\cot(\gamma + \theta) - \left(\frac{\pi}{2} - (\gamma + \theta)\right) + \frac{\cot(\gamma + \theta)\cos(\gamma + \theta)\sin(\theta)}{\sin(\gamma)}\right]. \tag{A.8}$$

References

[1] C. Mack et al., Fifty years of moore's law, IEEE Trans. Semicond. Manuf. 24 (2011) 202–207.
[2] Y. Shabany, Heat Transfer: Thermal Management of Electronics, CRC Press, 2009.
[3] T. Cotter, Principles and prospects for micro heat pipes, NASA STI/Recon Technical Report N 84 (1984) 29149.
[4] W.K. Jones, Y. Liu, M. Gao, Micro heat pipes in low temperature cofire ceramic (LTCC) substrates, IEEE Trans. Compon. Packag. Technol. 26 (2003) 110–115.
[5] M. Mochizuki, T. Nguyen, K. Mashiko, Y. Saito, T. Nguyen, V. Wuttijumnong, A review of heat pipe application including new opportunities, Front. Heat Pipes (FHP) 2 (2011).
[6] A. Faghri, Review and advances in heat pipe science and technology, J. Heat Transfer 134 (2012) 123001.
[7] H. Ma, G. Peterson, The minimum meniscus radius and capillary heat transport limit in micro heat pipes, J. Heat Transfer 120 (1998) 227–233.
[8] D. Reay, P. Kew, Heat Pipes, fifth ed., Butterworth-Heinemann, London, 2006.
[9] F.L. Chang, Y.M. Hung, The coupled effects of working fluid and solid wall on thermal performance of micro heat pipes, Int. J. Heat Mass Transfer 73 (2014) 76–87.
[10] D. Sugumar, K.K. Tio, The effects of working fluid on the heat transport capacity of a microheat pipe, J. Heat Transfer 131 (2009) 012401.
[11] W. Wu, G. Peterson, Investigation of the transient characteristics of a micro heat pipe, J. Thermophys. 5 (2) (1991) 129–134.
[12] D. Khrustalev, A. Faghri, Thermal analysis of a micro heat pipe, J. Heat Transfer 116 (1) (1994) 189–198.
[13] Y.M. Hung, K.K. Tio, Thermal analysis of a water-filled micro heat pipe with phase-change interfacial resistance, J. Heat Transfer 134 (2012) 112901.
[14] K.K. Tio, C.Y. Liu, K.C. Toh, Thermal analysis of micro heat pipes using a porous-medium model, Heat Mass Transfer 36 (2000) 21–28.
[15] Y.M. Hung, K.K. Tio, Analysis of microheat pipes with axial conduction in the solid wall, J. Heat Transfer 132 (2010) 071301.
[16] Y. Hu, J. Cheng, W. Zhang, R. Shirakashi, S. Wang, Thermal performance enhancement of grooved heat pipes with inner surface treatment, Int. J. Heat Mass Transfer 67 (2013) 416–419.
[17] Z. Huang, J. Zhang, J. Cheng, S. Xu, P. Pi, Z. Cai, X. Wen, Z. Yang, Preparation and characterization of gradient wettability surface depending on controlling Cu $(OH)_2$ nanoribbon arrays growth on copper substrate, Appl. Surf. Sci. 259 (2012) 142–146.
[18] A. Sommers, T. Brest, K. Eid, Topography-based surface tension gradients to facilitate water droplet movement on laser-etched copper substrates, Langmuir 29 (2013) 12043–12050.
[19] S. Daniel, M.K. Chaudhury, J.C. Chen, Fast drop movements resulting from the phase change on a gradient surface, Science 291 (2001) 633–636.
[20] K.M. Ashley, J.C. Meredith, E. Amis, D. Raghavan, A. Karim, Combinatorial investigation of dewetting: polystyrene thin films on gradient hydrophilic surfaces, Polymer 44 (2003) 769–772.
[21] S.H. Choi, B.Z. Newby, Micrometer-scaled gradient surfaces generated using contact printing of octadecyltrichlorosilane, Langmuir 19 (2003) 7427–7435.
[22] B. Babin, G. Peterson, D. Wu, Steady state modeling and testing of a micro heat pipe, J. Heat Transfer 112 (1992) 595–601.
[23] X. Du, T. Zhao, Analysis of film condensation heat transfer inside a vertical micro tube with consideration of the meniscus draining effect, Int. J. Heat Mass Transfer 46 (2003) 4669–4679.
[24] S.-C. Wong, Y.-C. Lin, Effect of copper surface wettability on the evaporation performance: tests in a flat-plate heat pipe with visualization, Int. J. Heat Mass Transfer 54 (2011) 3921–3926.
[25] C.-C. Hsu, P.-H. Chen, Surface wettability effects on critical heat flux of boiling heat transfer using nanoparticle coatings, Int. J. Heat Mass Transfer 55 (2012) 3713–3719.
[26] J. Longtin, B. Badran, F. Gerner, A one-dimensional model of a micro heat pipe during steady-state operation, J. Heat Transfer 116 (1994) 709–715.
[27] B. Suman, N. Hoda, Effect of variations in thermophysical properties and design parameters on the performance of a v-shaped micro grooved heat pipe, Int. J. Heat Mass Transfer 48 (2005) 2090–2101.
[28] S. Kim, J. Seo, K. Do, Analytical and experimental investigation on the operational characteristics and the thermal optimization of a miniature heat pipe with a groovedwick structure, Int. J. Heat Mass Transfer 46 (2003) 2051–2063.
[29] P. Ayyaswami, I. Catton, D. Edwards, Capillary flow in triangular grooves, J. Appl. Mech. 41 (1974) 332–336.
[30] A. Faghri, Performance characteristics of a concentric annular heat pipe: Part II-vapor flow analysis, J. Heat Transfer 111 (4) (1989) 851–857.
[31] E. Lemmon, M. McLinden, D. Friend, Thermophysical properties of fluid systems, NIST Chemistry Webbook, NIST Standard Reference Database 69 (2005).